Developmental Cell
Article

# SKI-1 and Furin Generate Multiple RGMa Fragments that Regulate Axonal Growth

Nardos G. Tassew,[1,2] Jason Charish,[1,2] Nabil G. Seidah,[4] and Philippe P. Monnier[1,2,3,*]
[1]Genetics and Development Division, Toronto Western Research Institute, MCL-6-415, 399 Bathurst Street, Toronto M5T 2S8, Ontario, Canada
[2]Department of Physiology
[3]Department of Ophthalmology
Faculty of Medicine, University of Toronto, Toronto M5S 1A8, Ontario, Canada
[4]Laboratory of Biochemical Neuroendocrinology, Clinical Research Institute of Montreal, Montreal H2W 1R7, Quebec, Canada
*Correspondence: pmonnier@uhnres.utoronto.ca
DOI 10.1016/j.devcel.2011.11.022

## SUMMARY

**The nervous system is enormously complex, yet the number of cues that control axonal growth is surprisingly meager. Posttranslational modifications amplify diversity, but the degree to which they are employed is unclear. Here, we show that Furin and SKI-1 combine with autocatalytic cleavage and a disulfide bridge to generate four membrane-bound and three soluble forms of the repulsive guidance molecule (RGMa). We provide in vivo evidence that these proprotein convertases are involved in axonal growth and that RGMa cleavage is essential for Neogenin-mediated outgrowth inhibition. Surprisingly, despite no sequence homology, N- and C-RGMa fragments bound the same Fibronectin-like domains in Neogenin and blocked outgrowth. This represents an example in which unrelated fragments from one molecule inhibit outgrowth through a single receptor domain. RGMa is a tethered membrane-bound molecule, and proteolytic processing amplifies RGMa diversity by creating soluble versions with long-range effects as well.**

## INTRODUCTION

Axonal outgrowth is precisely orchestrated during development to ensure correct connectivity within the nervous system (Tessier-Lavigne and Goodman, 1996). Surprisingly, however, there are a relatively limited number of known guidance proteins (Thanos and Mey, 2001). Posttranslational modification is one strategy to generate multiple activities from a single protein. In theory, complex proteolytic processing with alternate use of multiple specific cleavage sites could dramatically increase diversity (Zisman et al., 2007). Semaphorins, which have several cleavage sites, are one example (Adams et al., 1997), but the extent to which this strategy is utilized and the effects on activity, receptor specificity, and/or short (membrane-bound) versus long-range (soluble) effects are largely unknown.

The GPI-anchored protein RGMa is key to the development of various projections within the CNS and is thought to act solely as a membrane-bound protein (Monnier et al., 2002). Its activity is similar to that of the ephrins, as it inhibits retinal ganglion cell (RGC) outgrowth (Monnier et al., 2002). RGMa acts through the transmembrane receptor Neogenin, which is expressed in a high-temporal low-nasal gradient in RGC axons (Rajagopalan et al., 2004). In vitro, temporal axons that express Neogenin avoid RGMa-expressing cells, whereas Neogenin-deficient nasal axons are not affected by RGMa (Rajagopalan et al., 2004). In vivo, perturbation of the RGMa gradient in the optic tectum causes pathfinding mistakes for temporal fibers (Matsunaga et al., 2006). Thus, Neogenin and RGMa provide positional information for retinal axons invading the tectum. Besides its contribution to the establishment of the neuronal architecture, RGMa is a major impediment to neuronal regeneration. Strikingly, antibodies that block RGMa activity promote functional recovery after spinal cord injury (Hata et al., 2006). Thus, to optimize therapeutics that promote axonal regeneration it is critical to understand how RGMa contributes to the nonpermissive regenerative milieu of the CNS.

Current understanding of RGMa processing derives from studies in transfected COS-7 cells, but the in vivo cleavage pattern remains uncharacterized (Tassew et al., 2009). Here we show that RGMa processing is far more complex than originally thought. Thus, alternative cleavage by the Proprotein Convertases Subtilisin Kexin Isozyme-1 (SKI-1) and Furin generates multiple membrane-bound and soluble forms, and the resulting peptides have dramatically different potencies, including released forms. In stark contrast to nonmembrane-bound ephrins that do not influence axonal outgrowth, we show that soluble forms of RGMa are inhibitory. Unexpectedly, distinct RGMa products with no sequence homology operate through the same Fibronectin III (3-4) domains in Neogenin. As RGMs are implicated in many human disorders (Papanikolaou et al., 2004; Nohra et al., 2010), the discovery of multiple derivatives is expected to have important implications for therapeutic targeting.

## RESULTS

### Complex In Vivo RGMa Processing

We performed western blotting on membrane preparations under reducing (+DTT) and nonreducing conditions (-DTT) to allow analysis of the RGMa disulfide bridge. As reported,

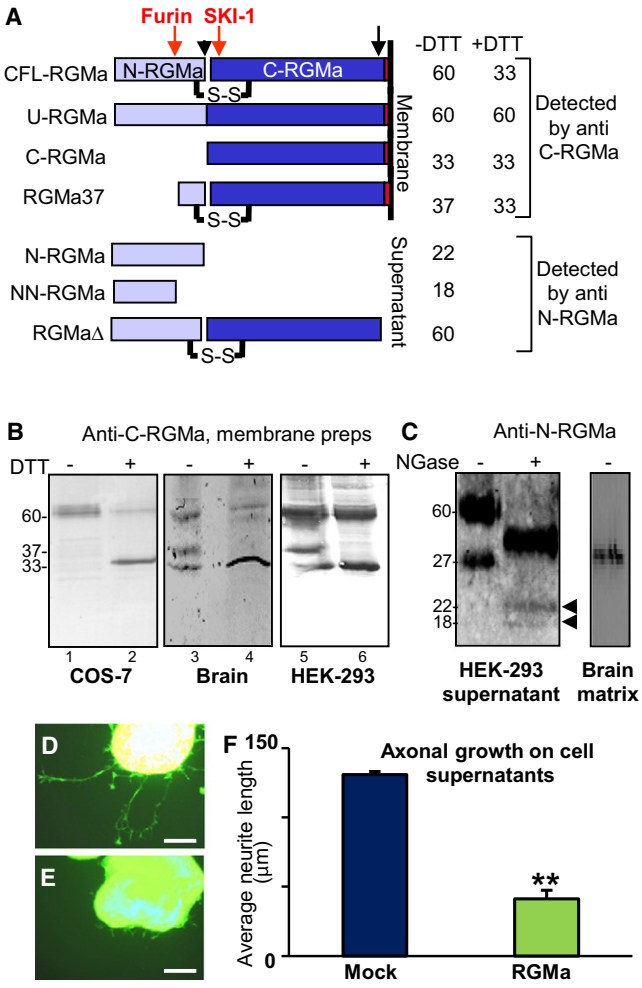


**Figure 1. Analysis of RGMa Processing**

(A) Schematic representation of the seven RGMa peptides identified in our analysis. In membranes under reducing (+DTT) or nonreducing (-DTT) conditions, an anti-C-RGMa revealed four RGMa fragments. In cell supernatant (-DTT), an anti-N-RGMa revealed that three RGMa fragments are released. Molecular weights are indicated on the right; UG unglycosylated. Black arrow head indicates autocatalytic cleavage site, black arrow represents known shedding cleavage site. Red arrows indicate calculated cleavage sites corresponding to soluble isoforms.

(B) Western blots with an anti-C-RGMa on membranes from RGMa-transfected COS-7 cells, the developing chick brain, and RGMa-transfected HEK293 cells. Analysis was performed under nonreducing conditions (-DTT) to preserve the disulfide bridge or under reducing conditions (+DTT). Under nonreducing conditions, one band is visible in COS-7 cells (60 kDa), whereas three bands (33, 37, and 60 kDa) are visible in chick brain and HEK293. Under reducing conditions two bands (33 and 60 kDa) are visible in membranes. This revealed four membrane-bound RGMa proteins in chick brain (represented in A; see also Figure S1).

(C) Western blots (-DTT) performed with an anti-N-RGMa on brain matrix extracts (urea 3M) revealed a 30 kDa band. In supernatants from RGMa-transfected HEK cells, two bands at 60 and 30 kDa are apparent. PNGaseF (NGase) treatment to remove N-glycosylations (UG) reduced the 60 kDa to a 45 kDa band and the 30 kDa to 22 and 18 KDa bands (arrow heads) (represented in A).

(D and E) Temporal retinal explants cultured on supernatants from cells transfected with control (Mock, D) or RGMa (E). Bar, 200 μm.

(F) Average axonal length was significantly shorter on supernatants from RGMa-transfected cells versus control (Mock; $^{**}p < 0.0005$). Data are average ± SEM from three independent experiments.

membranes from COS-7 cells transfected with RGMa contained a single 60 kDa protein, which DTT reduced to a 33 kDa C-terminal RGMa fragment ("C-RGMa") due to the presence of an autocatalytic cleavage site at residue 150 (Figures 1A and 1B, lanes 1 and 2; Tassew et al., 2009). Some of the 60 kDa band remained even after DTT treatment (Figure 1B, lane 2) suggesting that membranes contain both cleaved and uncleaved full-length RGMa (Figure 1A, CFL-RGMa and U-RGMa, respectively; Tassew et al., 2009). Whereas the C-terminal antibody only detected full-length 60 kDa protein on nonreduced COS-7 membranes (Figure 1B, lane 1), this protein plus the 33 kDa C-RGMa fragment and an unexpected 37 kDa species ("RGMa37") were observed on nonreduced membrane preparations from chick brain (Figure 1B, lane 3). Thus, in brain C-RGMa is present on membranes both as a linked heterodimer with N-RGMa (33 kDa+22 kDa), and on its own (33 kDa alone) (Figure 1B). The RGMa37 fragment disappeared after treatment with DTT (Figure 1B, lane 4) and must, therefore, arise from a second in vivo cleavage site located within the N-terminal part of RGMa, and consists of the 33 kDa C-RGMa fragment disulfide linked to a calculated 4 kDa N-RGMa fragment (Figure 1A). In summary, western blots with the C-terminal antibody suggest the presence of four distinct membrane-anchored RGMa proteins in vivo: CFL-RGMa (60 kDa), U-RGMa (60 kDa), C-RGMa (33 kDa), and RGMa37 (37 kDa).

## RGMa Is Processed into Soluble Proteins that Inhibit Axonal Growth

To further test and extend these conclusions we sought to identify cell lines which, unlike COS-7, recapitulate the more complex cleavage pattern seen in chick brain. Strikingly, western blotting with the C-terminal antibody on membranes from HEK293, and SH-SY5Y cells, but not COS-7 or DF1 cells, transfected with RGMa showed a pattern similar to the one observed in brain (Figure 1B, lanes 5 and 6; Figure S1 available online). While RGMa processing in HEK293 or SH-SY5Y cells did not seem as efficient as in the brain, these model cell lines could be used to study this process. The presence of two cleavage sites within the N-terminal domain should lead to the release of two small N-terminal fragments (Figure 1A, N-RGMa and NN-RGMa, respectively). Thus, we sought to identify these fragments in chick brain matrix extracts using N-terminal anti-RGMa antibodies. Surprisingly, we could only reveal the presence of one 30 kDa band that was bigger than any of the expected N-terminal fragments (Figure 1C). We extended this study to the medium of RGMa-transfected HEK293 cells and detected two RGMa proteins with apparent molecular masses of 60 and 30 kDa (Figure 1C, lane 1). The 60 kDa has been described before and results from RGMa shedding from the membrane (RGMaΔ) by a phospholipase (Hata et al., 2006) and may not be biologically relevant as it is not seen in brain matrices. The 30 kDa band was broad, so we surmised that it represented a glycosylated N-terminal fragment. To test this hypothesis, we removed N-glycosylations using PNGaseF and assessed its resulting molecular mass by western blot. Once unglycosylated (UG), the 60 kDa was reduced to one 45 kDa band whereas the 30 kDa resulted in 2 bands (18 and 22 kDa) that correspond to N-RGMa and NN-RGMa (Figure 1C). Thus, RGMa processing in HEK leads to the secretion of three soluble fragments: N-RGMa (30 kDa;

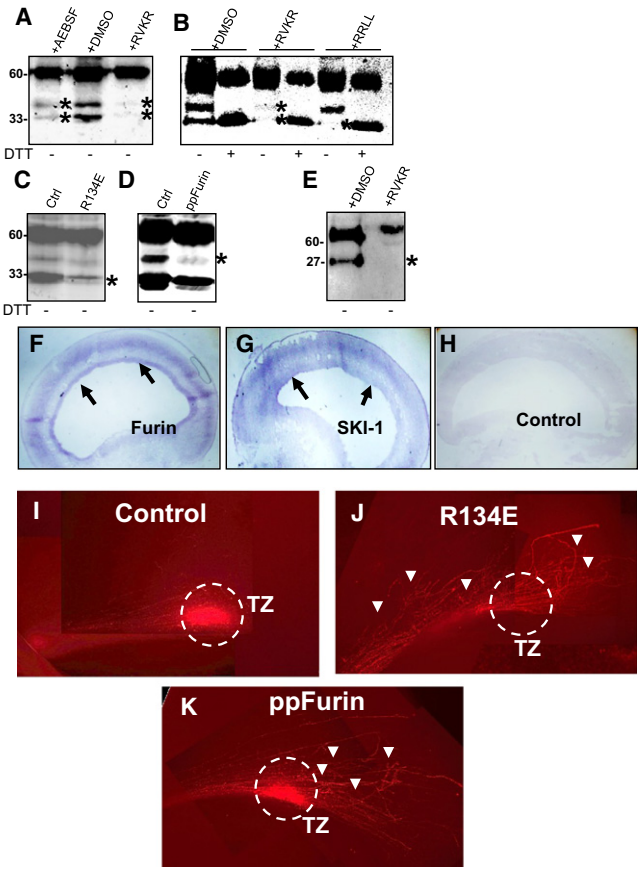


**Figure 2. Furin and SKI-1 Process RGMa and Are Involved in Pathfinding**

(A) RGMa-expressing cells were treated with the protease inhibitors AEBSF or RVKR, or DMSO (control) and membranes blotted. AEBSF and RVKR both strongly reduced RGMa cleavages, shown by the reduction of the 33 and 37 kDa bands (asterisks) (see also Figures S2A and S2B).

(B) RGMa-expressing cells were treated with RVKR or RRLL protease inhibitors or DMSO (control). Blots on membranes under reducing (+DTT) and nonreducing (-DTT) conditions show that RVKR inhibits the two cleavage events (asterisks), whereas the SKI-1 inhibitor RRLL inhibited generation of the 33 kDa protein only (asterisk). In the presence of DTT a 33 kDa band appears indicating that autocatalytic cleavage is not sensitive to treatments.

(C) RGMa was cotransfected with R134E or empty plasmid (control). In membranes, R134E strongly reduced formation of the 33 kDa protein (asterisk), confirming that it is the result of SKI-1 activity.

(D) RGMa was cotransfected with ppFurin or empty plasmid (Ctrl). ppFurin strongly reduced formation of the 37 kDa fragment, confirming that it results from Furin activity (see also Figure S2).

(E) RGMa-expressing cells were treated with DMSO (control) or RVKR and supernatants were blotted with anti-N-RGMa. RVKR suppressed release of N-terminal proteins (asterisk).

(F–H) In situ analysis demonstrated that Furin and SKI-1 are expressed in the tectum in RGMa-expressing radial glial cells (arrows). Controls (sense) did not show any staining (H).

(I) Injection of empty virus did not induce axonal phenotypes and all axons established terminal arbors within the terminal zone (TZ).

(J) Ectopic expression of a SKI-1 pro-form (R134E) induced axonal phenotypes with numerous fibers establishing arbors outside the TZ.

(K) Ectopic expression of ppFurin to neutralize Furin induced axonal phenotypes with numerous fibers establishing arbors outside the TZ (arrowheads).

22 kDa unglycosylated [UG]), NN-RGMa (30 kDa; 18 kDa [UG]) and RGMaΔ (60 kDa; 45 kDa [UG]).

To address the role of RGMa soluble proteins on growing axons, we cultured retinal explants in the presence of supernatant from cells that were either Mock transfected or transfected with full-length RGMa (Figures 1D–1F). Interestingly, cells grown on supernatant from RGMa-transfected HEK293 cells showed markedly reduced axonal growth (41.3 ± 6 μm) relative to those grown on media from Mock-transfected cells (131 ± 2.1 μm). Thus, RGMa-expressing cells release factors that hamper axonal growth.

## SKI-1 and Furin Process RGMa

The identification of 33 and 37 kDa species in membranes could be explained by two cleavage events, one within the N-terminal domain and one next to the autocatalytic site, respectively (Figure 1A). To identify the enzyme(s) that cleave(s) RGMa we treated cells with protease inhibitors. Of the many inhibitors tested, only AEBSF, a membrane permeable inhibitor for serine proteases, showed a significant reduction of RGMa cleavage (Figure 2A; Figure S2A). Interestingly, another non-membrane-permeable serine protease inhibitor (Aprotinin) did not show any reduction in cleavage. Because this indicates that RGMa is cleaved on its way toward the cell surface, we tested two inhibitors of transport from the endoplasmic reticulum (ER) to the Golgi (Seidah et al., 1999). Both Golgicide A and Brefeldin A did not have any effect on RGMa processing, indicating that it is cleaved within the ER (Figure S2B). This behavior corresponds to the one observed with Proprotein Convertases (PCs); hence, we tested the cell-permeable RVKR peptide, a broad inhibitor for PCs (Seidah and Chrétien, 1999). Membranes were analyzed by western blotting under nonreducing conditions, which showed that both the 33 and the 37 kDa bands, were completely abolished by RVKR treatments (Figure 2A). PCs normally require two arginines for cleavage; however, we could not identify any PC consensus sequence next to the autocatalytic site. Thus, we suspected that another PC that does not require arginines to induce cleavage was involved in RGMa processing. Because Subtilisin Kexin Isoenzyme-1 (SKI-1) does not require a basic residue at the cleavage site (Pasquato et al., 2006), we tested whether specific SKI-1 inhibition with the cell-permeable RRLL peptide inhibitor could prevent RGMa processing. Indeed, this peptide completely abolished formation of the 33 kDa band but not the 37 kDa suggesting that SKI-1 mediates generation of the former protein (Figure 2B). In all cases, the presence of DTT resulted in the formation of the 33 kDa band indicating that treatments with these inhibitors did not suppress the autocatalytic cleavage event (Figure 2B).

To confirm that SKI-1 is involved in RGMa processing, we expressed a prosegment inhibitor of this enzyme (R134E; Figure 2C; Pullikotil et al., 2004) together with RGMa. Here again, SKI-1 inhibition dramatically reduced formation of the 33 kDa band (Figure 2C). Next, we tested whether Furin processes RGMa by using a Furin-prosegment inhibitor construct that specifically prevents Furin cleavage (ppFurin; Zhong et al., 1999). Here, the formation of the 37 kDa species was blocked suggesting the involvement of Furin (Figure 2D). This was confirmed by the fact that soluble RGMa formed a 37 kDa band when treated by purified Furin (Figure S2). Finally, to

confirm that Furin and SKI-1 generate soluble N-terminal peptides, we studied cell supernatants after treatment with RVKR. As expected, the 60 kDa band but not the 30 kDa band was released by RGMa-expressing cells (Figure 2E).

In summary, RGMa processing is far more complex than previously appreciated; thus, autocatalytic cleavage and proteolytic cleavage by SKI-1 and Furin generate seven distinct species (Figure 1A). Furthermore, RGMa is N-glycosylated, adding to the complexity of its posttranslational modifications (Figure 1).

## SKI-1 and Furin Are Involved in Axonal Guidance

Although Furin activates Semaphorins (Adams et al., 1997), its in vivo function on growing axons remains unclear. We therefore investigated the role of Furin and SKI-1 on visual paths. First, we studied expression of these proteins using in situ hybridization in the optic tectum. Our data revealed that both proteins are expressed in RGMa-expressing radial glia cells (Figures 2F–2H), which fits the idea that they may be involved in retino-tectal pathfinding. Next, we performed ectopic-expression of SKI-1-(R134E) and Furin-inhibitors (ppFurin) in developing chicks (Figures 2I–2K) using the RCAS viral vector and studied retinal tracts from the eye to the optic tectum using DiI tracing. As expected, both SKI-1 and Furin inhibitions induced axonal phenotypes within the tectum. We observed that many fibers failed to target the terminal zone and arborized randomly within the tectum, when compared to controls (Figures 2I–2K). ppFurin induced aberrant paths in all embryos (n = 8) and 70% (7 of 10) of the R134E embryos but none of the controls (n = 6) displayed phenotypes. Furin and SKI-1 may regulate the activity of other guidance molecule. Indeed, Furin activates Semaphorins, which are critical for the growth of many axons (Adams et al., 1997). While these experiments do not directly show that RGMa cleavage by Furin and SKI-1 regulates axonal paths, they are consistent with that model and provide in vivo evidence that these enzymes play a critical role in the regulation of axonal growth.

## RGMa Cleavage Is Required for Neogenin Binding and Outgrowth Inhibition

The above insights raise important questions regarding the biological relevance of each of the multiple cleavage sites and the relative activity of each resulting peptide. First we examined whether RGMa cleavage is required for interaction with Neogenin. For this, we generated mutations next to the auto-catalytic cleavage site (D149A, H151A) and showed that these mutations altered all cleavage events (Figure 3B). These mutations did not change RGMa processing toward the cell surface (Figure S3). We then performed an ELISA assay in which Neogenin-AP interacts with membranes from COS-7 cells transfected with RGMa constructs (Figures 3A–3C; Figures S3A–S3C). In agreement with previous observations, wt RGMa interacted with Neogenin-AP (Rajagopalan et al., 2004), however, the two RGMa mutants did not interact with Neogenin (Figures 3B and 3C). Binding of membrane-bound RGMa to Neogenin is believed to be necessary for RGMa to exert its inhibition on axonal growth (Rajagopalan et al., 2004). To address this issue, we tested whether the RGMa mutants (D149A, H151A) inhibit axonal growth of Neogenin-expressing temporal axons. As controls, we cultured nasal axons that express lower amounts of Neogenin. As expected, temporal explants grown on wt RGMa membranes extended shorter axons (197.6 ± 7.5 μm) when compared to the otherwise long axons on Mock membranes (407.9 ± 16.7 μm) (Figures 3D and 3E). Outgrowth on U-RGMa mutants was 70.8% (335.7 ± 11.7 μm; $p < 0.0001$; D149A) and 82.2% longer (360 ± 6.1 μm; $p < 0.0001$; H151A) than on wt RGMa (Figures 3D and 3E). Because they express lower amounts of Neogenin, the reduction in length for nasal axons on wtRGMa versus control was lesser than the one observed with temporal axons (Figure 3E).

To confirm that catalytic cleavage is essential for Neogenin-mediated inhibition, we studied neurite growth on Neogenin-expressing NIE-115 cells (Endo and Yamashita, 2009). RGMa-containing membranes inhibited NIE-115 neurite extension compared to control Mock-transfected membranes (Figures 3F and 3G). This effect was Neogenin-dependent as it was suppressed when cells were treated with a Neogenin shRNA (Figure 3G; Figure S3), but not with control shRNA (Figure 3F and 3G). Here again, noncleavable mutants did not inhibit growth (Figures 3F and 3G).

We next examined the effect of RGMa cleavage on axonal pathfinding and performed ectopic expression of wt RGMa and U-RGMa (H151A). As expected, tectal infection with a vector that expressed wt RGMa induced strong pathfinding mistakes (Figure 3H). In 100% of the embryos (13 of 13), we observed that axons established terminal arbors outside the predicted terminal zone (TZ) indicating that RGMa overexpression perturbed pathfinding. In contrary, no obvious axonal phenotype was observed when H151A was overexpressed in the tectum (Figure 3I). Here, 89% (8 of 9) of the embryos displayed normal behavior with all fibers terminating their growth within the predicted TZ.

Together, these data demonstrate that RGMa catalytic processing is required for interaction with Neogenin and the resulting neurite/axon growth inhibition.

## C-RGMa on Its Own Is Sufficient for Neogenin Binding and Growth Inhibition

It has been assumed that C-RGMa on its own is sufficient to inhibit axonal growth (Rajagopalan et al., 2004). This notion derives from experiments that were performed before the identification of a disulfide bridge between N- and C-RGMa (Tassew et al., 2009), and remains to be tested. C-RGMa (33 kDa) is poorly targeted to the cell surface when expressed on its own (Tassew et al., 2009). Thus, to target C-RGMa to the cell surface, we developed a construct (C-RGMa$^{TEV}$) in which the original autocatalytic cleavage site between N- and C-RGMa was replaced by a TEV cleavage site (Phan et al., 2002; Figure 4A; Figure S4). In ELISAs, either RGMa$^{wt}$ or C-RGMa$^{TEV}$ membrane preparations bound Neogenin-AP, but notably C-RGMa$^{TEV}$ ($Kd$ = 6.8 nM) had a higher affinity than RGMa$^{wt}$ ($Kd$ = 11.96 nM; Figures 4C–4E). These data suggested that C-RGMa may inhibit axonal growth more effectively that the full-length protein. Indeed, membranes containing C-RGMa$^{TEV}$ inhibited temporal axons more potently than RGMa$^{wt}$ (Figures 4F and 4G). As expected, outgrowth from nasal axons was significantly higher, which is consistent with a role for Neogenin as the receptor (Figure 4G). To confirm that Neogenin mediated C-RGMa inhibition,

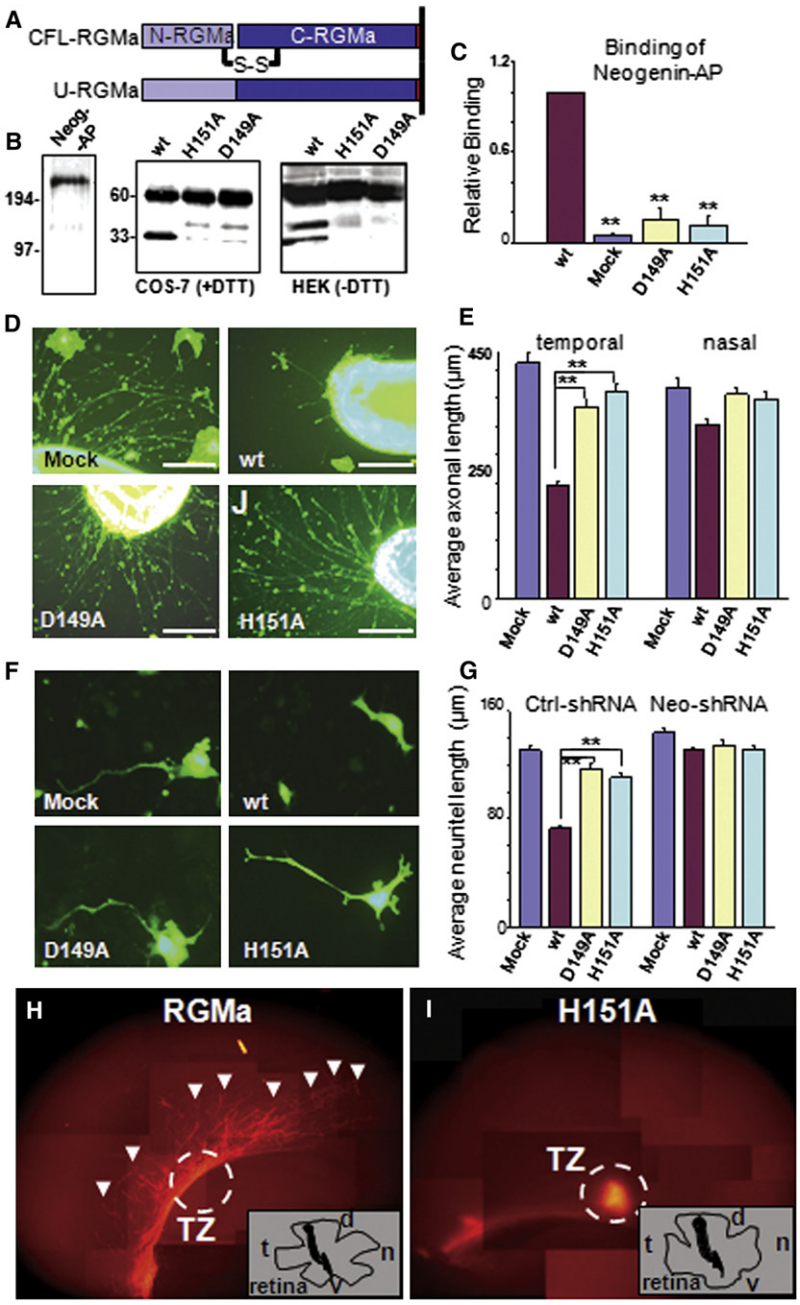


**Figure 3. RGMa Cleavage Is Required for RGMa Inhibition through Neogenin**

(A) RGMa proteins tested.

(B) Expression of Neogenin-AP (Neo-AP) and RGMa constructs in COS-7 and HEK293 cells. The introduction of a single mutation (H151A, D149A) next to autocatalytic cleavage site (aa 150) abolished cleavage in COS-7 cells. The same mutations abolished all cleavage events in HEK293 cells.

(C) Microtiter plates were coated with transfected COS-7-membranes and Neogenin-AP binding studied. Binding is abolished in noncleavable mutants (D149A, H151A) versus wtRGMa (wt; see also Figures S3A–S3C).

(D) Temporal explants grown on Mock, wtRGMa (wt), and noncleavable mutants (D149A; H151A) membranes. Axonal growth is reduced on wtRGMa versus Mock and mutants. Bar, 150 μm.

(E) In four independent experiments, mutation of the cleavage site abolished RGMa inhibition on temporal axons (**$p < 0.05$). Nasal axons that express less Neogenin were less inhibited.

(F) NIE-115 cells were grown on Mock, wtRGMa (wt), D149A, and H151A membranes, after transfection with GFP plasmid plus a control shRNA (Ctrl-shRNA) or a Neogenin shRNA (Neo-shRNA). NIE-115 cells transfected with Ctrl-shRNA extend shorter neurites on wtRGMa versus Mock, D149A, and H151A. Bar, 30 μm.

(G) D149A and H151A significantly increased length (**$p < 0.001$) compared to wtRGMa. Neogenin silencing with Neo-shRNA suppressed wtRGMa inhibition. All data are average ± SEM from three independent experiments (see also Figure S3).

(H) Ectopic expression of RGMa induced axonal phenotypes with numerous fibers establishing arbors outside the Terminal Zone (TZ; arrowheads).

(I) Ectopic expression of H151A did not induce axonal phenotypes and all axons established terminal arbors within the TZ.

we performed silencing experiments using NIE-115 cells on C-RGMa$^{TEV}$, RGMa$^{wt}$, and Mock-transfected membranes. In agreement with retinal axon data, C-RGMa$^{TEV}$ and RGMa$^{wt}$ significantly hampered neurite growth, an effect that vanished in the presence of Neogenin shRNA but not control shRNA (Figures 4H and 4I).

To rule out the possibility that the activity in C-RGMa$^{TEV}$ membranes resulted from unwashed N-RGMa fragments, we sought to identify the C-RGMa domain that interacts with Neogenin (Figure 4J). Using an interaction assay, we identified a domain spanning aa residues 182–271 that is sufficient for interaction with Neogenin (Figures 4J and 4K). In outgrowth experiments, C-RGMa$^{182-271}$ strongly inhibited temporal fibers (Figure S4B). A lesser effect was obtained on nasal fibers suggesting that this effect is mediated by Neogenin (Figure 4L). To assess the function of C-RGMa$^{182-271}$ on retino-tectal map formation we performed its ectopic expression in the chick tectum (Figures S4B–S4E). In 90% (9 of 10) of the embryos, C-RGMa$^{182-271}$ expression resulted in aberrant pathfinding (Figures 4M–4O). Together, these data demonstrate that C-RGMa on its own is sufficient for Neogenin interaction and inhibition of axonal growth.

## Three RGMa Soluble Proteins Inhibit Axonal Outgrowth via Neogenin

Because RGMa is GPI anchored and has the same action on growing fibers as ephrins (Drescher et al., 1997), it has been assumed that only membrane-bound RGMa inhibits axons (Monnier et al., 2002). To our knowledge, the release of three soluble RGMa proteins (RGMaΔ, N-RGMa, and NN-RGMa; Figure 1A) has not been reported before; we therefore sought to determine their function using purified proteins on growing

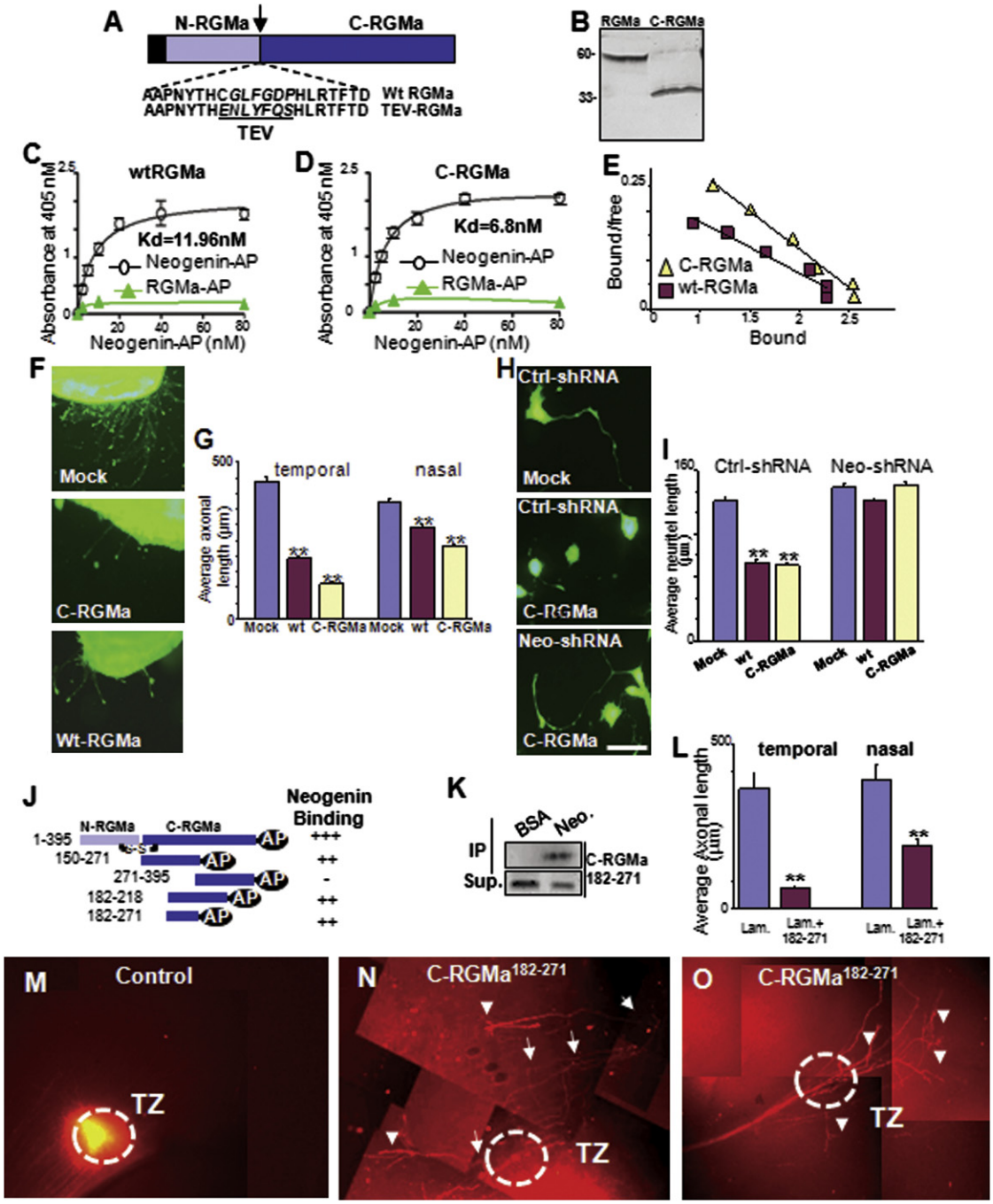


**Figure 4. C-RGMa Induces Neogenin-Mediated Inhibition**

(A) Representation of RGMa with a TEV site.

(B) Under nonreducing conditions, RGMa appears as a 60 kDa band, whereas RGMa-TEV is cleaved by TEV and only C-RGMa (33 kDa) is apparent.

(C and D) Neogenin-AP binds saturably to wtRGMa (C) and C-RGMa (D). Binding of Neogenin-AP or RGMa-AP to microtiter wells coated with C-RGMa and wtRGMa membranes. Neogenin-AP binding to BSA was less than 5% of these levels. Calculated *Kd* of Neogenin-AP is indicated. Data are from six determinations.

(E) Scatchard of Neogenin-AP binding (see also Figure S4).

(F) Temporal-axon growth was reduced on wtRGMa and C-RGMa membranes versus Mock. Bar, 150 μm.

(G) C-RGMa and wtRGMa significantly reduced length (**$p < 0.001$) of temporal axons. Nasal axons were inhibited to a lesser extent. Data are average ± SEM from four independent experiments.

(H) NIE-115 cells transfected with Ctrl-shRNA + GFP extend shorter neurites on C-RGMa versus Mock. Transfection of Neo-shRNA + GFP restored growth. Bar, 30 μm.

(I) C-RGMa and wtRGMa reduced NIE-115-neurite length (**$p < 0.0001$) in Ctrl-shRNA cells. Neo-shRNA suppressed this inhibition. Data are average ± SEM from three independent experiments.

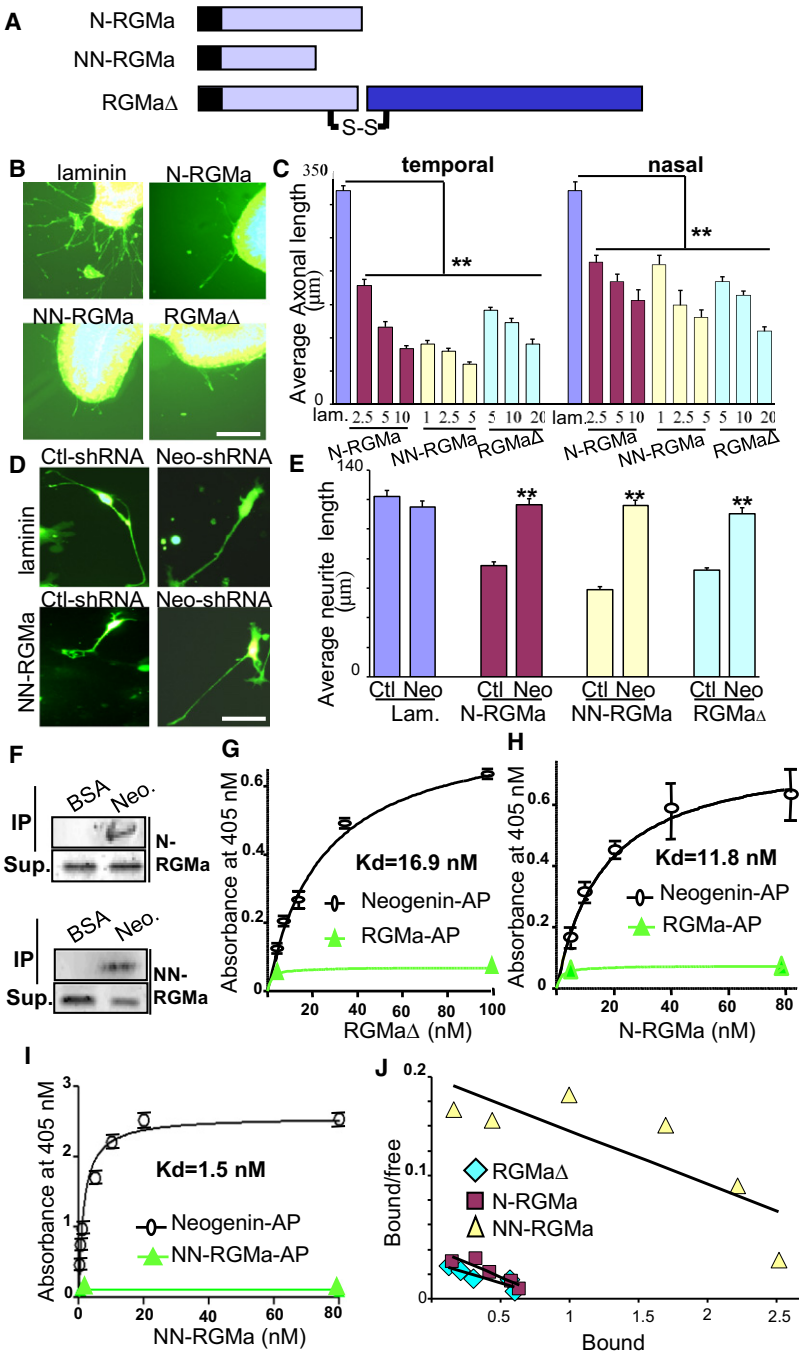


**Figure 5. Soluble RGMa Proteins Display Neogenin-Dependent Inhibition**

(A) RGMa proteins tested.

(B) Temporal explants on laminin, laminin+5 μg/ml N-RGMa, 2.5 μg/ml NN-RGMa, and 10 μg/ml RGMaΔ. The three RGMas inhibited growth. Bar, 200 μm.

(C) RGMa proteins significantly decreased growth (**$p < 0.0001$). Proteins displayed a concentration-dependent effect, NN-RGMa having the strongest effect. Nasal axons were less inhibited. Data are average ± SEM from four independent experiments. Bar, 150 μm.

(D) NIE-115 cells on laminin, laminin+5 μg/ml NN-RGMa, with control shRNA (Ctrl-shRNA)+GFP or a Neogenin shRNA (Neo-shRNA) +GFP. Cells transfected with Ctrl-shRNA extended shorter neurites on laminin+NN-RGMa, compared to laminin. Neo-shRNA restored growth. Bar, 40 μm.

(E) RGMaΔ, N-RGMa, and NN-RGMa inhibited growth. Neo-shRNA increased the average neurite-length on N-RGMa, NN-RGMa, and RGMaΔ, when compared to Ctrl-shRNA (**$p < 0.05$). Data are average ± SEM from four independent experiments.

(F) Supernatants (Sup.) from cells transfected with N-RGMa or NN-RGMa were pulled down (IP) by Neogenin- but not BSA-coated beads.

(G–I) Neogenin-AP (2 μg/well) bound saturably to purified RGMaΔ (G), N-RGMa (H), and NN-RGMa (I). RGMa-AP (2 μg/well) did not bind to RGMa proteins. Neogenin-AP binding to BSA was less than 5% of these levels. *Kd* of Neogenin-AP is indicated.

(J) Scatchard plot of RGMa proteins binding.

Data are average ± SEM from four to eight determinations (see also Figure S5).

fibers (Figure S5). Strikingly, RGMaΔ, N-RGMa, and NN-RGMa significantly inhibited retinal fibers in a concentration-dependent manner (Figures 5B and 5C). All proteins restricted outgrowth and displayed a greater activity on temporal versus nasal fibers, indicating that their receptor is present in higher quantities on temporal fibers. Remarkably, the shorter NN-RGMa fragment was the most potent inhibitor of outgrowth as 1 μg/ml of this protein led to 71% inhibition of temporal fibers, similar to that obtained with 10 μg/ml of N-RGMa (74%) or 20 μg/ml of RGMaΔ (72%; Figure 5C).

Because all fragments displayed stronger effect on temporal versus nasal axons, we tested whether Neogenin mediates their inhibition. NIE-115 cells expressing a control shRNA extended shorter processes on RGMaΔ, N-RGMa, and NN-RGMa compared to laminin alone, which was suppressed in cells expressing Neogenin-shRNA (Figures 5D and 5E). Here also, NN-RGMa (5 μg/ml) was more potent than N-RGMa (10 μg/ml) and RGMaΔ (20 μg/ml; Figure 5E). Together with the temporal/nasal difference described above (Figure 5C), these data show that Neogenin mediates inhibition by N-RGMa,

(J) Binding study of RGMas to Neogenin. RGMas were expressed as AP fusion proteins and tested in ELISA plates coated with the extracellular domain of Neogenin (binding; –, base line; ++, > 5 × base line; +++, > 10 × base line).

(K) Supernatants (Sup.) from cells transfected with C-RGMa$^{182-271}$ were pulled down (IP) by Neogenin- but not BSA-coated beads.

(L) C-RGMa$^{182-271}$ reduced axonal length (**$p < 0.005$). Nasal axons were less inhibited. Data are average ± SEM from three independent experiments.

(M–O) Ectopic expression of RGMa$^{182-271}$ induced pathfinding errors in the visual pathway. In control experiments (M), all the fibers targeted the terminal zone (TZ), whereas in RGMa$^{182-271}$ experiments fibers displayed aberrant paths (arrows) and connections (arrow heads) outside the TZ (N and O).

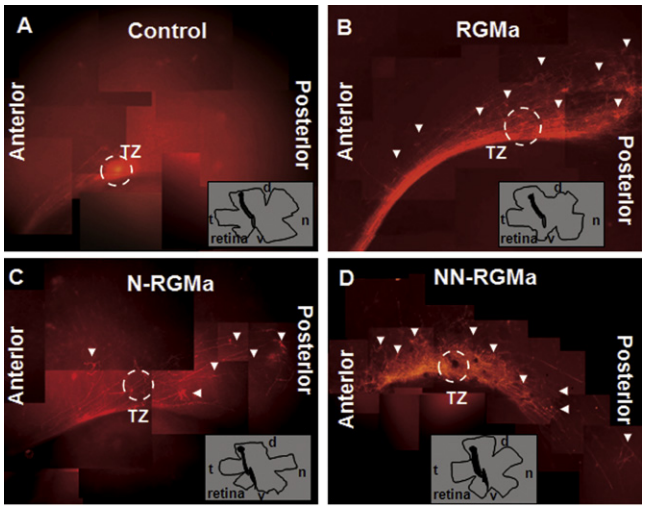


E

| | -TZ | AT | PT | Ab |
|---|---|---|---|---|
| Control (n=8) | 0% | 0% | 12% | 0% |
| RGMa (n=10) | 60% | 70% | 70% | 30% |
| N-RGMa (n=10) | 40% | 70% | 60% | 40% |
| NN-RGMa (n=12) | 25% | 42% | 100% | 58% |

**Figure 6. Overexpression of Soluble RGMa Proteins Perturbs Axonal Pathfinding in the Embryonic Chicken Visual System**

At embryonic day 1.5 (E1.5), RCAS-virus (control) and RCAS-RGMa (positive control), RCAS-N-RGMa, and RCAS-NN-RGMa were injected into the developing optic tectum. At E15, a DiI crystal was placed in the temporal retina to label fibers.

(A) In control experiments, all axons converge toward a well-defined terminal zone (TZ).

(B–D) Infections with RGMa, N-RGMa, and NN-RGMa-expressing RCAS-virus, induced (1) the absence of terminal zone, (2) the presence of ectopic anterior terminations, (3) aberrant turns and ectopic posterior terminations. All errors are indicated by arrow heads. The insets represent a drawing of the flat-mounted retina to indicate the location of the DiI crystal in a dorsotemporal position of the retina and the path of axons toward the optic fissure. t, temporal; d, dorsal; v, ventral; n, nasal. The hypothetical TZ is represented in each panel (see also Figure S6).

(E) Quantification of axonal phenotypes. -TZ, no terminal zone; AT, ectopic anterior terminations; PT, ectopic posterior terminations; Ab, aberrant turns.

NN-RGMa, and RGMaΔ (Figures 5D and 5E). Unexpectedly, this revealed that, unlike ephrins, soluble RGMa proteins inhibit axonal growth.

## RGMa Soluble Proteins Display Various Affinities to Neogenin

These data prompted us to examine whether Neogenin interacts directly with soluble N-terminal RGMa proteins. We performed pull down on supernatants from cells expressing N-RGMa or NN-RGMa, and observed coimmunoprecipitation with Neogenin- but not BSA-coated beads (Figure 5F), raising the possibility that they directly interact with Neogenin. Because RGMa proteins displayed varying potency, we determined binding affinities to Neogenin (Figures 5G–5J). Purified RGMaΔ bound to Neogenin-AP with a *Kd* of 16.9 nM (Figure 5G). The interaction was specific because RGMa-AP did not bind detectably to RGMa fragments and Neogenin-AP did not bind to BSA-coated wells. In the same assay, N-RGMa exhibited a higher affinity to Neogenin-AP with a calculated *Kd* of 11.8 nM (Figure 5H). Strikingly, the affinity of Neogenin for NN-RGMa was substantially greater with a *Kd* of 1.5 nM, 11-fold greater than the soluble full-length RGMaΔ protein (Figures 5I and 5J). A similar study in which NN-RGMa-AP and N-RGMa-AP interact with Neogenin-coated plates was performed and confirmed NN-RGMa's higher affinity (*Kd* = 1.2 nM) for Neogenin compared to N-RGMa (*Kd* = 8.2 nM; Figure S5). These affinities correlate with the inhibitory action of RGMa proteins on outgrowth (Figure 5C).

## N-RGMa and NN-RGMa Perturb Pathfinding In Vivo

RGMa gain- and loss-of-function experiments indicate that it is a key protein for the establishment of visual maps (Matsunaga et al., 2006). However, these experiments did not establish which RGMa fragment(s) is (are) involved in pathfinding. The fact that secreted RGMa proteins may control retinal axon pathfinding was unexpected as RGMa was believed to (1) function similar to ephrins, which require polymerization in membranes to guide axons (Egea and Klein, 2007) and (2) use its C-terminal portion to inhibit axonal growth. To assess a role of N-RGMa, and NN-RGMa during retinal-map formation, we performed ectopic expression of these proteins in the developing tectum using viral-mediated expression (Figure S6). In controls (empty virus), retinal fibers directly targeted the predicted terminal zone (TZ; Figure 6A). However, when N-RGMa and NN-RGMa were overexpressed (Figure 5) pathfinding was greatly perturbed (Figures 6B–6D). Abnormal axonal paths included terminations outside the TZ, aberrant turns within the optic tectum, as well as the absence of a clear TZ (Figures 6B–6D). In situ hybridization has demonstrated that expression patterns of other guidance molecules are not affected by ectopic expression of RGMa (Matsunaga et al., 2006), thus, the axon-targeting phenotype arises from an effect of overexpression of RGMa constructs and not from a modification of other proteins. In summary, ectopic expression of soluble RGMa N-terminal proteins indicates that they are involved in the formation of visual maps.

## C- and N-RGMa Proteins Interact with the Same Neogenin FNIII(3-4) Domain

We next sought to identify the Neogenin domain(s) with which C- and N-RGMa proteins interact. The extracellular portion of Neogenin contains four Immunoglobulin like (4Ig) and six Fibronectin type III (6FNIII) domains (Figure 7A). It has been reported that 6FNIII interacts with full-length RGMa (Rajagopalan et al., 2004). Using 6FNIII-AP, we showed that C- and N-RGMa proteins interact with 6FNIII (Figure 7A). Next, we sought to identify which sub-region of the 6FNIII domain(s) interact with N- and C-RGMa. To do so, we generated Neogenin constructs that contain only some of the six FNIII domains (Figure 7A). In interaction assays, the FNIII (2-5) domains bound to all C- and N-RGMa proteins, which contrasted with domains 1–3 and 4–6 that did not interact with any RGMa protein (Figure 7A). To further refine the location of the binding motif, we generated a construct that only contains the FNIII(3-4) domains, and showed that this segment was sufficient for binding to each one of the RGMa

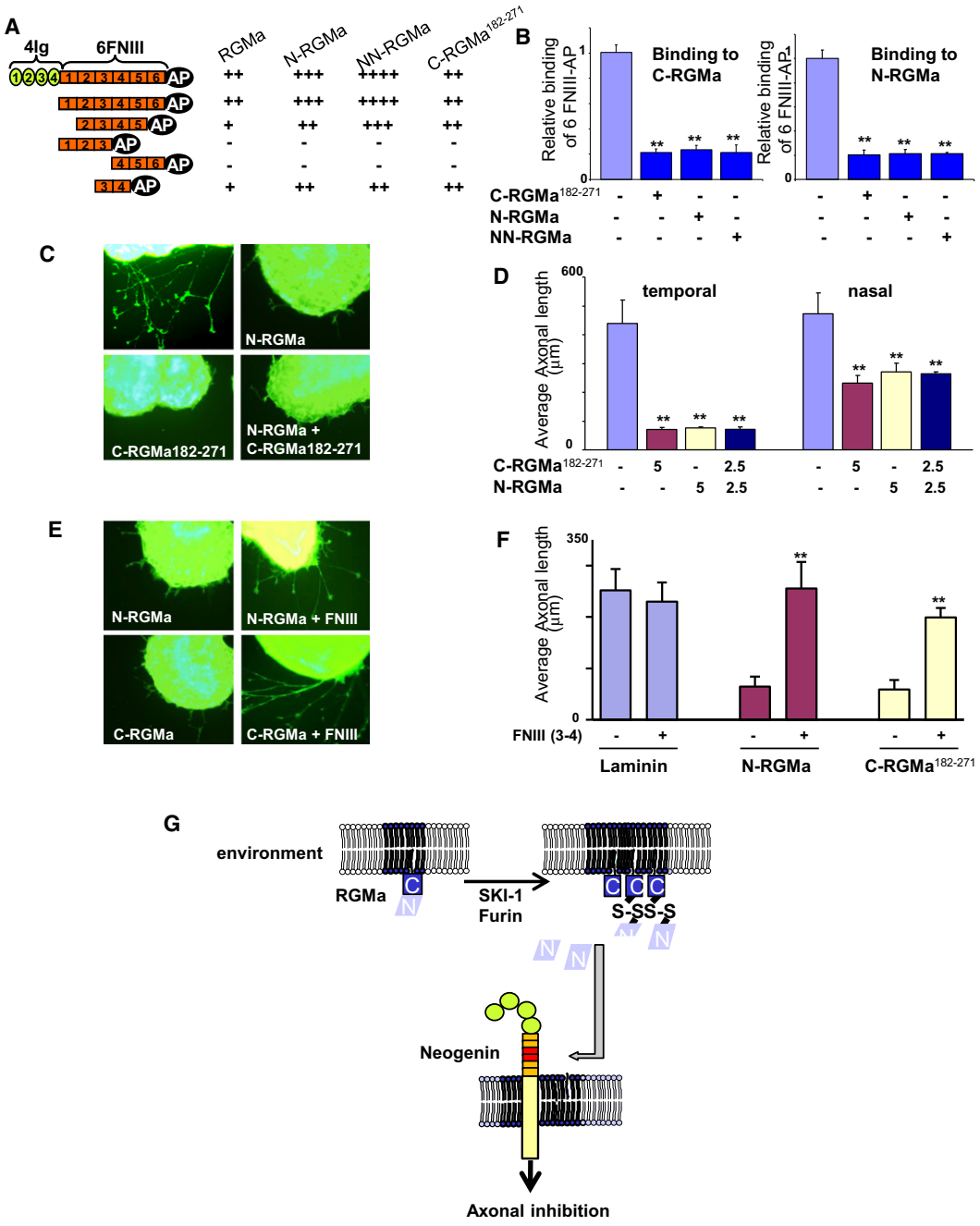


**Figure 7. N- and C-RGMa Inhibit Axonal Outgrowth by Binding to the Same Neogenin Domain**

(A) The extracellular portion of Neogenin consists of four immunoglobulin-like (4Ig) and six fibronectin type III (6FNIII) domains. ELISA plates were coated with RGMa proteins and binding of Neogenin-AP was studied. (Binding; −, base line; + > 2 × base line; ++ > 3 × base line; +++ > 5 × base line). The three to four fibronectin (FNIII[3-4]) domains sufficed for binding to RGMa proteins.

(B) ELISA plates were coated with N-RGMa or C-RGMa and binding of 6FNIII-AP was assessed after incubation with C-RGMa$^{182-271}$, N-RGMa or NN-RGMa. Preincubation with either N- or C-RGMa proteins altered 6FNIII-AP binding to both C- and N-RGMa proteins.

(C) Temporal axons grown on combinations of N- and C-RGMa.

(D) Quantification of axonal growth on 5 μg/ml of N-RGMa, 5 μg/ml C-RGMa$^{182-271}$, and 2.5 μg/ml N-RGMa + 2.5 μg/ml C-RGMa$^{182-271}$ (**$p < 0.005$). Data are average ± SEM from three independent experiments.

(E) Temporal axons grown on N- and C-RGMa in the presence or absence of FNIII(3-4).

(F) Quantification of axonal growth on laminin, laminin + 2.5 μg/ml of N-RGMa, and laminin + 2.5 μg/ml C-RGMa$^{182-271}$ in the presence or absence of FNIII(3-4). FNIII(3-4) significantly restored axonal growth on N-RGMa, and C-RGMa$^{182-271}$ (**$p < 0.01$). Data are average ± SEM from three independent experiments.

(G) Model for RGMa action on Neogenin. SKI-1 and Furin digest RGMa into C- and N-terminal proteins all interact with the fibronectin domain (3-4) of Neogenin (red) to inhibit axonal growth.

proteins (Figure 7A). Because C- and N-RGMa fragments bind to the same Neogenin subdomain, we tested whether they interfere with each other. In these experiments, we assessed 6FNIII-AP binding to C- or N-RGMa after incubation with either one of these proteins. As expected, preincubation of Neogenin with C-RGMa abolished binding to C-RGMa. Interestingly, preincubation with N-RGMa also inhibited binding of Neogenin to C-RGMa, indicating that C- and N-RGMa interfere in their binding to Neogenin (Figure 7B). In agreement with these data, binding to N-RGMa was also altered when Neogenin was preincubated to either C- or N-terminal fragments (Figure 7B). Next we studied the effect of the combined presence of RGMa proteins on axonal growth. When axons were grown on equimolar concentrations of either N-RGMa (5 μg/ml), C-RGMa$^{182-271}$ (5 μg/ml, these proteins have the same apparent molecular weight) or N-RGMa (2.5 μg/ml) + of C-RGMa$^{182-271}$ (2.5 μg/ml), all treatments resulted in inhibitions that did not significantly differ from each other (Figures 7C and 7D). This represents the third indication that both N- and C-fragments act through FNIII(3-4).

To further assess the role of FNIII(3-4) in RGMa inhibition, we tested its function-blocking capability. Retinal axons were grown on RGMa proteins in the presence of 1 μg/ml of FNIII(3-4). Remarkably, the presence of this fragment restored axonal growth on RGMaΔ, N-RGMa, and C-RGMa, indicating that it blocked the inhibitory activities of these proteins on retinal axons (Figures 7E and 7F). Together, these data represent a unique example in which two unrelated domains of a same guidance molecule inhibit axonal growth through interaction with the same receptor region.

## DISCUSSION

RGMa has critical roles in axonal growth, cell differentiation, apoptosis, neuronal regeneration, and bone development (Monnier et al., 2002; Matsunaga et al., 2004, 2006; Hata et al., 2006; Zhou et al., 2010). Our data revealed that proteolytic cleavage together with the formation of a disulfide bridge generate 4 membrane-bound and three soluble RGMa species. This level of complexity was not expected as it was believed that only full-length RGMa, in which RGMa is either uncleaved or its N- and C-RGMa fragments remain attached by a disulfide bridge, is expressed in vivo (Tassew et al., 2009). We studied the activity of individual RGMa proteins and showed that all cleaved protein products inhibit neurite growth via Neogenin, while the full-length uncleaved membrane-bound RGMa is inactive. Hence, proteolysis is required for RGMa activity. Furthermore, we show that two Proprotein Convertases (PCs), namely Furin and SKI-1 are involved in RGMa processing and generate N-terminal soluble and C-terminal membrane-bound proteins with different inhibitory activities. Surprisingly, RGMa fragments with no apparent sequence homology all interacted with the same Fibronectin domains in Neogenin to inhibit axonal growth.

Regulation of the activity of extracellular proteins by proteolytic cleavage is an emerging theme within the CNS (Adams et al., 1997). PCs form a family of nine proteinases with a large array of functions within the CNS (Seidah and Chrétien, 1999). Some members of the family have been shown to process extracellular proteins thereby regulating axonal growth. For instance, Furin activates members of the Semaphorin family (Adams et al., 1997). Similarly, PC5/6A cleaves the neural adhesion molecule L1, an event that appears important for L1-dependent neurite growth of cerebellar neurons (Kalus et al., 2003). Thus far, SKI-1 has not been shown to play any role within the CNS. Therefore, this study uncovers an unexpected aspect of SKI-1 function in the CNS. SKI-1 knockout mice die at embryonic days 2–3 (Mitchell et al., 2001) and that of Furin die of heart defect at embryonic day 11 (Roebroek et al., 1998). Thus, a function for these proteins could not be assessed within the developing CNS. Using local perturbation of SKI-1 and Furin function in the developing tectum, we generated evidence that both proteins regulate axonal growth in vivo.

RGMa and ephrin-A5,-A2 are GPI-anchored proteins that guide retinal fibers (Monnier et al., 2002; Drescher et al., 1997). Thus, they have both been assumed to function as membrane-bound cues. Here, however, we show that soluble RGMa proteins also strongly inhibit fiber growth. This is in stark contrast to ephrins, which require oligomerization in membrane clusters to be functionally active (Egea and Klein, 2007). Activity of ephrins is also regulated by proteolytic processing. For instance, ephrin-A2 is cleaved by Kuzbanian after binding to its receptor, a mechanism that leads to axon detachment and termination of signaling (Hattori et al., 2000). Strikingly, release of RGMa from the membrane has the opposite effect since uncleaved membrane-bound protein is inactive, and proteolysis creates active soluble RGMa proteins. Thus, our data invoke an unexpected mechanism of action for RGMa in which the combination of long (soluble) and short (membrane-bound) range guidance regulates topographic mapping.

Surprisingly, unrelated N- and C-terminal fragments inhibit axonal growth via the same Fibronectin domains in Neogenin. At first sight this result confirms a recent study in which we showed that both domains are involved in retino-tectal pathfinding (Tassew et al., 2009). Because in COS-7 cells, N- and C-RGMa are linked to each other by a disulfide bridge, the logical interpretation was that RGMa simultaneously requires N- and C-RGMa for interaction with Neogenin. We now postulate that pathfinding toward the optic tectum can be controlled by independent and unrelated N- and C-terminal RGMa fragments. It is known for other proteins such as Nogo or NG2 that multiple distinct regions might contribute to their inhibitory activity (Oertle et al., 2003). However, unlike RGMa, each one of these regions uses a distinct receptor to transmit its inhibitory activities (Oertle et al., 2003). Ephrins have two domains that interact with the Eph receptors; however, only one of these domains has an inhibitory action on growing fibers (Carvalho et al., 2006). Slit2 is processed into several peptides, however only the D2 inhibitory domain binds to robo-receptor whereas the other inhibitory domain D4 interacts with heparin sulfate (Seiradake et al., 2009). Thus, to our knowledge, RGMa represents the first example in which multiple inhibitory fragments from a single ligand regulate axonal growth through the same receptor domain.

As well as controlling connections within the developing CNS, RGMa is involved in neurodegenerative diseases. Thus, it is a major impediment to neuronal regeneration and antibodies that neutralize C-RGMa promote regeneration (Hata et al., 2006). Moreover, there is growing evidence that RGMa is a key player in multiple sclerosis (Muramatsu et al., 2011; Nohra et al., 2010). In the light of our new data, multiple

RGMa-fragments may contribute to the negative environment that hampers regeneration following CNS injury. Optimal approaches to deactivate RGMa should target all inhibitory C- and N-terminal fragments. The RGM family is implicated in the disease hemochromatosis (Papanikolaou et al., 2004), and accordingly it will be important to determine whether the complex processing we uncovered here affects the activity of other RGM proteins.

## EXPERIMENTAL PROCEDURES

### Cloning, Expression, and Purification

All RGMa constructs were cloned in pSectag2B vector (Invitrogen) with an N-terminal His-tag. They were then transferred to RCAS BP(B) vector for viral production. SKI-1 and ppFurin were cloned in the bicistronic eGFP-containing pIRES vector (Invitrogen) as we published before (Pullikotil et al., 2004).

C-RGMa-TEV was cloned by inserting a TEV cleavage site between N-RGMa and C-RGMa. Membranes were prepared from transfected cells, washed and resuspended in 1× TEV buffer and cleaved with AcTEV protease (Invitrogen) ON at 4°C. Membranes were washed to remove the cleaved N-terminal part, and resuspended in PBS.

Soluble proteins were purified using Ni-NTA agarose (Invitrogen) and dialyzed in PBS. Anti-His (QIAGEN) and anti-RGMa (8B6; Tassew et al., 2009) were used.

### Binding Assay

A 96-well plate was coated with (1) poly-L-lysine (100 μl, 10 μg/ml) and (2) membrane suspensions (100 μl) adjusted to an OD of 0.1 (at 220 nm) were added to the wells. Plates were then centrifuged at 3,000 rpm (15 min at 4°C), blocked with 5% BSA for 1 hr, and different concentrations of AP-tagged proteins were added for 3 hr. Wells were washed with PBS, incubated at 65°C for 1 hr to deactivate endogenous AP and developed with 1 mg/ml pNPP.

For binding assay, wells were coated with purified proteins (3 hr at room temperature [RT]), and blocked with 5% BSA (1 hr), followed by incubation with AP-tagged proteins (2 μg/well; 3 hr at RT). To quantify the binding, absorbance at 405 nm was measured by using a microplate reader (EL 311SX, Bio-TEK Instruments Inc.). *Kd* and scatchard plots were obtained after fitting the data using a nonlinear curve fit by GraphPad Prism 5 software.

### Neogenin Silencing and Neurite Outgrowth

Mouse Neogenin shRNA and control shRNA were gifts from Dr. Yamashita T. NIE-115 cells which endogenously express Neogenin were cotransfected with shRNA and GFP. Twenty-four hours later, cells were plated on coverslips coated with membranes from Mock, wtRGMa, D149A and H151A (OD of 0.1 at 220 nm). Alternatively, cells were cultured on molar equivalent amounts of soluble proteins, RGMaΔ (20 μg/ml), N-RGMa (10 μg/ml) and NN-RGMa (5 μg/ml). Cells were differentiated in 2% DMSO and neurite length was measured 48 hr later.

### Retinal Explants Outgrowth Assay

Glass coverslips were coated with 10 μg/ml poly-L-lysine, treated with laminin (10 μg/ml), and membrane preparations from transfected cells were added and centrifuged for 15 min at 3,000 × g and 4°C. Alternatively, different concentrations of soluble proteins mixed with laminin (10 μg/ml) were added to the coverslips and incubated for 3 hr at RT. Explants from the temporal and Nasal retina were then added to either membrane-or protein-coated surfaces in DMEM F-12 media (2% chick serum, 10% FBS) and incubated (37°C, 5% $CO_2$) for 18 hr. Explants were fixed in 4%PFA, permeablized with 0.1% Triton X-100, stained with Alexa488-fluor-phalloidin and viewed under a fluorescence microscope (Zeiss). The number and length of fibers were then quantified using Image Pro 5.0. Only explants which displayed growth were considered.

### Cell Treatments

HEK cells transfected with RGMa and grown for 24 hr were treated with 50 μM RVKR, 300 μM AEBSF (ENZO life science), and 50 μM RRLL (BACHEM) for 12 hr before membranes or supernatants were processed.

### Pull-Down Assay

Proteins were coupled to activated-CNBr Sepharose (Pharmacia). Beads were then blocked with 100 mM Tris-HCl, (pH 8) and washed. Supernatants from transfected cells were added to coupled beads for 2 hr at RT. Beads were then washed six times with PBS +0.02% Tween 20, and SDS loading buffer was added. Samples were boiled and subjected to western blotting.

### Preparation of Viral Stocks

DF1 cells (DSHB) were transfected with RCAS constructs using lipofectamine 2000 (Invitrogen). Cultures were expanded and supernatants were collected, pooled, and concentrated by centrifugation (21,000 rpm, 2 hr) in a SW 28 rotor (Beckman). Viral titer was determined by infecting DF1 cells with serial dilutions and staining for the gag protein (AMV-3C2 Ab; DSHB). Titers of 1 × $10^8$ IU/ml were used for infections.

### In Ovo Injection and DiI Tracing

Eggs (White Leghorn) were incubated at 38°C in high-humidity. At E1.5 viral solution (viral titers of 1 × $10^8$ IU/ml) was injected in the tectum. At E15, a small DiI crystal (Molecular Probes) was placed in the temporodorsal part of the right eye. At E17, tecta were fixed in 4% PFA. DiI tracing was viewed under a fluorescent microscope (Olympus BX61) after cutting the tecta in half. Digital Images were taken and processed using Photoshop (Adobe).

### Statistical Analysis

Quantifications were done for binding and outgrowth assays from at least three independent experiments. Statistical analysis was performed using ANOVA by XLSTAT. Results are expressed as the average ± SEM.

## SUPPLEMENTAL INFORMATION

Supplemental Information includes six figures and Supplemental Experimental Procedures and can be found with this article online at doi:10.1016/j.devcel.2011.11.022.

## ACKNOWLEDGMENTS

We thank Drs. Rod Bremner, John G. Flanagan, Jeffrey Wrana, James Eubanks, Marty Steinbach, and Jeffrey Hurwitz for constant support and discussions. We Thank Dr. T. Yamashita for providing shRNA constructs. This work was supported by the Heart and Stroke Foundation of Ontario (grant NA7067 to P.P.M.), the Canadian Institutes for Health Research (grant MOP106666 to P.P.M.), and grant MOP44363 and Canada Chair 216684 (to N.G.S.).

Received: February 3, 2011
Revised: September 19, 2011
Accepted: November 21, 2011
Published online: February 13, 2012

## REFERENCES

Adams, R.H., Lohrum, M., Klostermann, A., Betz, H., and Püschel, A.W. (1997). The chemorepulsive activity of secreted semaphorins is regulated by furin-dependent proteolytic processing. EMBO J. *16*, 6077–6086.

Carvalho, R.F., Beutler, M., Marler, K.J.M., Knöll, B., Becker-Barroso, E., Heintzmann, R., Ng, T., and Drescher, U. (2006). Silencing of EphA3 through a cis interaction with ephrinA5. Nat. Neurosci. *9*, 322–330.

Drescher, U., Bonhoeffer, F., and Müller, B.K. (1997). The Eph family in retinal axon guidance. Curr. Opin. Neurobiol. *7*, 75–80.

Egea, J., and Klein, R. (2007). Bidirectional Eph-ephrin signaling during axon guidance. Trends Cell Biol. *17*, 230–238.

Endo, M., and Yamashita, T. (2009). Inactivation of Ras by p120GAP via focal adhesion kinase dephosphorylation mediates RGMa-induced growth cone collapse. J. Neurosci. *29*, 6649–6662.

Hata, K., Fujitani, M., Yasuda, Y., Doya, H., Saito, T., Yamagishi, S., Mueller, B.K., and Yamashita, T. (2006). RGMa inhibition promotes axonal growth and recovery after spinal cord injury. J. Cell Biol. *173*, 47–58.

Hattori, M., Osterfield, M., and Flanagan, J.G. (2000). Regulated cleavage of a contact-mediated axon repellent. Science *289*, 1360–1365.

Kalus, I., Schnegelsberg, B., Seidah, N.G., Kleene, R., and Schachner, M. (2003). The proprotein convertase PC5A and a metalloprotease are involved in the proteolytic processing of the neural adhesion molecule L1. J. Biol. Chem. *278*, 10381–10388.

Matsunaga, E., Tauszig-Delamasure, S., Monnier, P.P., Mueller, B.K., Strittmatter, S.M., Mehlen, P., and Chédotal, A. (2004). RGM and its receptor neogenin regulate neuronal survival. Nat. Cell Biol. *6*, 749–755.

Matsunaga, E., Nakamura, H., and Chédotal, A. (2006). Repulsive guidance molecule plays multiple roles in neuronal differentiation and axon guidance. J. Neurosci. *26*, 6082–6088.

Mitchell, K.J., Pinson, K.I., Kelly, O.G., Brennan, J., Zupicich, J., Scherz, P., Leighton, P.A., Goodrich, L.V., Lu, X., Avery, B.J., et al. (2001). Functional analysis of secreted and transmembrane proteins critical to mouse development. Nat. Genet. *28*, 241–249.

Monnier, P.P., Sierra, A., Macchi, P., Deitinghoff, L., Andersen, J.S., Mann, M., Flad, M., Hornberger, M.R., Stahl, B., Bonhoeffer, F., and Mueller, B.K. (2002). RGM is a repulsive guidance molecule for retinal axons. Nature *419*, 392–395.

Muramatsu, R., Kubo, T., Mori, M., Nakamura, Y., Fujita, Y., Akutsu, T., Okuno, T., Taniguchi, J., Kumanogoh, A., Yoshida, M., et al. (2011). RGMa modulates T cell responses and is involved in autoimmune encephalomyelitis. Nat. Med. *17*, 488–494.

Nohra, R., Beyeen, A.D., Guo, J.P., Khademi, M., Sundqvist, E., Hedreul, M.T., Sellebjerg, F., Smestad, C., Oturai, A.B., Harbo, H.F., et al. (2010). RGMA and IL21R show association with experimental inflammation and multiple sclerosis. Genes Immun. *11*, 279–293.

Oertle, T., van der Haar, M.E., Bandtlow, C.E., Robeva, A., Burfeind, P., Buss, A., Huber, A.B., Simonen, M., Schnell, L., Brösamle, C., et al. (2003). Nogo-A inhibits neurite outgrowth and cell spreading with three discrete regions. J. Neurosci. *23*, 5393–5406.

Papanikolaou, G., Samuels, M.E., Ludwig, E.H., MacDonald, M.L., Franchini, P.L., Dubé, M.P., Andres, L., MacFarlane, J., Sakellaropoulos, N., Politou, M., et al. (2004). Mutations in HFE2 cause iron overload in chromosome 1q-linked juvenile hemochromatosis. Nat. Genet. *36*, 77–82.

Pasquato, A., Pullikotil, P., Asselin, M.C., Vacatello, M., Paolillo, L., Ghezzo, F., Basso, F., Di Bello, C., Dettin, M., and Seidah, N.G. (2006). The proprotein convertase SKI-1/S1P. In vitro analysis of Lassa virus glycoprotein-derived substrates and ex vivo validation of irreversible peptide inhibitors. J. Biol. Chem. *281*, 23471–23481.

Phan, J., Zdanov, A., Evdokimov, A.G., Tropea, J.E., Peters, H.K., 3rd, Kapust, R.B., Li, M., Wlodawer, A., and Waugh, D.S. (2002). Structural basis for the substrate specificity of tobacco etch virus protease. J. Biol. Chem. *277*, 50564–50572.

Pullikotil, P., Vincent, M., Nichol, S.T., and Seidah, N.G. (2004). Development of protein-based inhibitors of the proprotein of convertase SKI-1/S1P: processing of SREBP-2, ATF6, and a viral glycoprotein. J. Biol. Chem. *279*, 17338–17347.

Rajagopalan, S., Deitinghoff, L., Davis, D., Conrad, S., Skutella, T., Chedotal, A., Mueller, B.K., and Strittmatter, S.M. (2004). Neogenin mediates the action of repulsive guidance molecule. Nat. Cell Biol. *6*, 756–762.

Roebroek, A.J., Umans, L., Pauli, I.G., Robertson, E.J., van Leuven, F., Van de Ven, W.J., and Constam, D.B. (1998). Failure of ventral closure and axial rotation in embryos lacking the proprotein convertase Furin. Development *125*, 4863–4876.

Seidah, N.G., and Chrétien, M. (1999). Proprotein and prohormone convertases: a family of subtilases generating diverse bioactive polypeptides. Brain Res. *848*, 45–62.

Seidah, N.G., Mowla, S.J., Hamelin, J., Mamarbachi, A.M., Benjannet, S., Touré, B.B., Basak, A., Munzer, J.S., Marcinkiewicz, J., Zhong, M., et al. (1999). Mammalian subtilisin/kexin isozyme SKI-1: A widely expressed proprotein convertase with a unique cleavage specificity and cellular localization. Proc. Natl. Acad. Sci. USA *96*, 1321–1326.

Seiradake, E., von Philipsborn, A.C., Henry, M., Fritz, M., Lortat-Jacob, H., Jamin, M., Hemrika, W., Bastmeyer, M., Cusack, S., and McCarthy, A.A. (2009). Structure and functional relevance of the Slit2 homodimerization domain. EMBO Rep. *10*, 736–741.

Tassew, N.G., Charish, J., Chestopalova, L., and Monnier, P.P. (2009). Sustained in vivo inhibition of protein domains using scFv recombinant antibodies and its application to dissect RGMa activity on retinal axon outgrowth. J. Neurosci. *29*, 1126–1131.

Tessier-Lavigne, M., and Goodman, C.S. (1996). The molecular biology of axon guidance. Science *274*, 1123–1133.

Thanos, S., and Mey, J. (2001). Development of the visual system of the chick. II. Mechanisms of axonal guidance. Brain Res. Brain Res. Rev. *35*, 205–245.

Zhong, M., Munzer, J.S., Basak, A., Benjannet, S., Mowla, S.J., Decroly, E., Chrétien, M., and Seidah, N.G. (1999). The prosegments of furin and PC7 as potent inhibitors of proprotein convertases. In vitro and ex vivo assessment of their efficacy and selectivity. J. Biol. Chem. *274*, 33913–33920.

Zhou, Z., Xie, J., Lee, D., Liu, Y., Jung, J., Zhou, L., Xiong, S., Mei, L., and Xiong, W.C. (2010). Neogenin regulation of BMP-induced canonical Smad signaling and endochondral bone formation. Dev. Cell *19*, 90–102.

Zisman, S., Marom, K., Avraham, O., Rinsky-Halivni, L., Gai, U., Kligun, G., Tzarfaty-Majar, V., Suzuki, T., and Klar, A. (2007). Proteolysis and membrane capture of F-spondin generates combinatorial guidance cues from a single molecule. J. Cell Biol. *178*, 1237–1249.